ACS ES&T Air

Open Access

pubs.acs.org/estair

Article

Sector-, Season-, and Country-Specific NO_2-Associated Health Benefits from NO_x Emission Reductions

Published as part of ACS ES&T Air special issue "John H. Seinfeld Festschrift".

Patrick Wiecko,* Daven K. Henze, and M. Omar Nawaz

Cite This: *ACS EST Air* 2025, 2, 700−709

Read Online

ACCESS | Metrics & More | Article Recommendations | Supporting Information

ABSTRACT: Long-term exposure to NO_2 is associated with elevated risks for pediatric asthma and premature death. Despite national policies targeting NO_2's main source, NO_x emissions, its global health burden remains high. Here, we use the air quality model GEOS-Chem adjoint with TROPOspheric Monitoring Instrument (TROPOMI)-based satellite downscaling to estimate that long-term NO_2 exposure is responsible for 2.07 (95% CI 0.91−2.70) million pediatric asthma cases and 1.98 (95% CI 0.52−2.86) million deaths globally in 2019. We attribute these to anthropogenic NO_x emissions by sector, country, and season using the adjoint model and provide a recommendation for the most impactful sector and season for NO_x emission controls in each G20 country. Discrepancies exist between the health benefits incurred by emission reductions and the emission sector distributions, particularly in countries with emitters adjoining population centers. For example, we find that, if Russian anthropogenic NO_x emissions were reduced uniformly by 10% across all sectors, the energy sector, 31% of annual NO_x emissions, would account for 47% of pediatric asthma and 49% of premature death health benefits. The season in which these emission reductions occur also affects the magnitude of the health benefit, as seen by the fact that Russian wintertime NO_x emission reductions alone are responsible for approximately one-third of the annual health benefits for each health outcome. We present the unique results for each of the G20 members to showcase how a country's NO_x emission reductions can be most impactful in reducing the global NO_2-associated health burden.

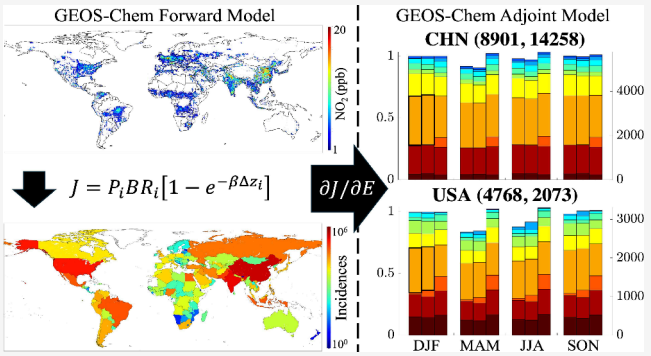

KEYWORDS: *Air Quality, Nitrogen Oxides, GEOS-Chem, Adjoint Modeling, Health, Emissions*

1. INTRODUCTION

Of the many species that contribute to air pollution, nitrogen dioxide (NO_2) stands out as not only a precursor of harmful pollutants like ozone (O_3) and fine particulate matter ($PM_{2.5}$) but also a species linked to illnesses itself. Exposure to NO_2 is a statistically significant risk factor for respiratory and cardiometabolic morbidity, birth defects, and acute mortality,[1] with asthma development in children[2] and premature deaths in older populations[1] being the two most studied health outcomes globally. Achakulwisut et al.[3] estimated the global burden of pediatric asthma attributed to NO_2 exposure in 2015 to be 4.0 (95% CI 1.8−5.2) million incidences, accounting for 13% (95% CI 6−16%) of all pediatric asthma incidences, but their NO_2 concentration data set, based on land use regression (LUR), tended to overestimate exposure in rural areas. Anenberg et al.[4] updated this LUR data set by correcting for this positive rural bias using satellite NO_2 data and found 1.85 (95% CI 0.93−2.83) million pediatric asthma incidences are associated with NO_2 exposure in 2019, accounting for 8.5% (95% CI 4.3−12.8%) of all incidences. Although an improvement, the NO_2 exposure metrics used by Anenberg et al.[4] remain significantly uncertain over the United States (US), Canada, and the European Union (EU) due to reliance on LUR estimates with frequently sparse monitoring data and an older satellite data set (SCIAMACHY and GOME-2) with a coarser resolution than more modern products.

NO_2 primarily originates from nitrogen oxide (NO_x) emissions, which largely occur as a result of high-temperature combustion. These emissions are predominantly anthropogenic in origin with only around 16% of global annual NO_x emissions coming from natural sources. Transportation emits the greatest share at around 36% of all anthropogenic NO_x emissions in 2020, with industrial combustion accounting for

Received: January 13, 2025
Revised: March 6, 2025
Accepted: March 10, 2025
Published: March 19, 2025

20% and energy generation and extraction operations making up 14%.[5] The process of determining which NO_x emissions are most directly responsible for NO_2 exposure is influenced by several factors that must be considered when identifying sources of the NO_2 health burden, including nonlinearities in NO_2's photochemical loss processes and transport via reservoir species, which necessitates the use of a chemical transport model.

To further understand the regional contributions to the global NO_2 health burden and better quantify the role of emissions from specific sectors and seasons, here, we seek to apportion the 2019 global health burden associated with modeled NO_2 exposure, with improved horizontal resolution using satellite downscaling, to changes in anthropogenic NO_x emissions. We first quantify the 2019 global health burden of pediatric asthma and premature deaths associated with NO_2 exposure using the chemical transport model GEOS-Chem and apply satellite downscaling to improve the exposure estimate's accuracy. While other health end points are also associated with NO_2 exposure,[6,7] pediatric asthma and premature death are the focus of our study as these two have readily available baseline incidence rates by country, provided by the Global Burden of Disease study,[8] and strong evidence for association with NO_2 exposure.[1] While pediatric asthma has a causal relationship with NO_2 exposure, many acute symptoms have only been locally correlated with NO_2 exposure.[9] Moreover, the nature of our study, annual NO_2 concentrations using annual oversampled satellite data available only once daily, lends itself better to chronic studies over acute ones, which require more confidence in estimating hourly time series of NO_2 concentrations for precise exposure calculations. We then calculate the contributions of anthropogenic NO_x emissions by economic sector, country, and season to the annual global health burden using the adjoint model. We focus our analysis on the Group of Twenty (G20) countries due to their dominant share of the global population (67%[10]) and anthropogenic NO_x emissions (65%[5]). While prior adjoint modeling studies have examined regional source attributions of health burdens to NO_x emissions,[11,12] we present here the first adjoint-based sensitivity analysis of the global NO_2-associated health burden.

2. METHODS

2.1. Quantifying the Global NO_2-Associated Health Burden. Calculating the 2019 global health burdens associated with NO_2 exposure requires population age, baseline incidence of an outcome, and the attributable fraction of an outcome to NO_2 exposure. We use age-stratified, globally gridded population data from the WorldPop database's unconstrained global mosaics at the 1 × 1 km resolution,[10] which we regridded to a 0.01° × 0.01° resolution. Country-scale baseline health outcome incidence rates in 2019 are from the 2021 Global Burden of Disease (GBD) Study[8] and are aligned to the stratified 5-year age distributions of the WorldPop database for the affected ages of pediatric asthma (0−19) and mortality (30−80+). For each health outcome, we use a log−linear exposure response function to calculate the associated relative risk.[1,2] The number of health outcomes associated with NO_2 exposure are then calculated as

$$O_h = \sum_{i\in D}\sum_{g\in G} P_i^g B_i^g (1 - e^{-\beta_h \Delta z_i}) \quad (1)$$

where O_h is the global burden of specific health outcome h attributable to NO_2 exposure, P_i^g is the population in grid cell i within the global domain D belonging to age group g out of all age groups G, B_i^g is the baseline incidence rate of a health outcome in cell i for age group g, β_h is the concentration response factor for each health outcome, and Δz_i is the annual average surface NO_2 concentration above the counterfactual (i.e., the concentration level below which no outcomes are assumed to occur). For the values of β, we use a relative risk of 1.26 (95% uncertainty interval 1.1−1.37) per 10 ppb NO_2 increment for pediatric asthma risk associated with NO_2 exposure and 1.04 (95% confidence interval 1.01−1.06) per 10 $\mu g/m^3$ NO_2 (converted to 5.32 ppb NO_2) for mortality risk due to NO_2 exposure, and the counterfactual associated with pediatric asthma and premature death was 2 ppb NO_2 and 0 ppb NO_2, respectively.[1,2] Because all-cause mortality can also be associated with exposure to other pollutants, the relative risk used for premature deaths associated with NO_2 exposure was derived while controlling for O_3 and $PM_{2.5}$ exposure to remove any double-counting of deaths.[1]

2.2. Calculating the Annual-Average Surface NO_2 Concentration. Annual average surface NO_2 concentrations (z_i) are calculated using the forward model component of GEOS-Chem adjoint v35n at a global 2° × 2.5° resolution, which are downscaled to a 0.01° × 0.01° horizontal grid using NO_2 satellite data. We retrieve the tropospheric component of the total vertical NO_2 column from the TROPOspheric Monitoring Instrument (TROPOMI) v2.4.0 and spatiotemporally average them from January 1st, 2019 through December 31st, 2019 using the oversampling method from Sun et al.[13] These oversampled tropospheric NO_2 columns are then used in a downscaling procedure outlined in Cooper et al.[14] and updated to follow a modeling framework by Nawaz et al.[12] in which 24-h annual-average simulated NO_2 columns are combined with the annual-average oversampled TROPOMI columns from 2019 to calculate the annual average surface NO_2 concentration at the fine 0.01° × 0.01° resolution. Equations 2 and 3 summarize the procedure as

$$z_i = \kappa_i \left(\frac{\nu_i \Omega_I - \Omega_I^{FT}}{\Omega_I - \Omega_I^{FT}}\right)\left(\frac{S_{NO_2,I}}{\Omega_I}\right)\Omega_I^* \quad (2)$$

$$\kappa_i = \begin{cases} 1, & \text{if } \Omega_i < 10^{14} \\ (1 - w_i) + \chi_i w_i, & \text{if } 10^{14} < \Omega_i < 10^{17} \\ \chi_i, & \text{if } \Omega_i > 10^{17} \end{cases} \quad (3)$$

where z_i is the annual average surface NO_2 concentration at the 0.01° × 0.01° resolution (denoted by the subscript i), Ω_I is the modeled annual-averaged tropospheric NO_2 column with the * superscript denoting it as the active variable for differentiation at the 2° × 2.5° resolution (denoted by the subscript I), Ω_I^{FT} is the portion of the model column above the planetary boundary layer in the free troposphere, ν_i is the lower column variability defined as the ratio of a TROPOMI column in fine grid cell i to the TROPOMI column averaged over the coarse grid cell I of which the prior column lies within, and $S_{NO_2,I}$ is the annual average surface NO_2 concentration at the lowest vertical model level. κ_i, a scaling factor dependent on the tropospheric column abundance, varies with respect to w_i, a linear interpolation of the column abundance between the given abundance thresholds (the source of the discontinuity in κ_i), and χ_i, the ratio of

https://doi.org/10.1021/acsestair.5c00012
ACS EST Air 2025, 2, 700−709

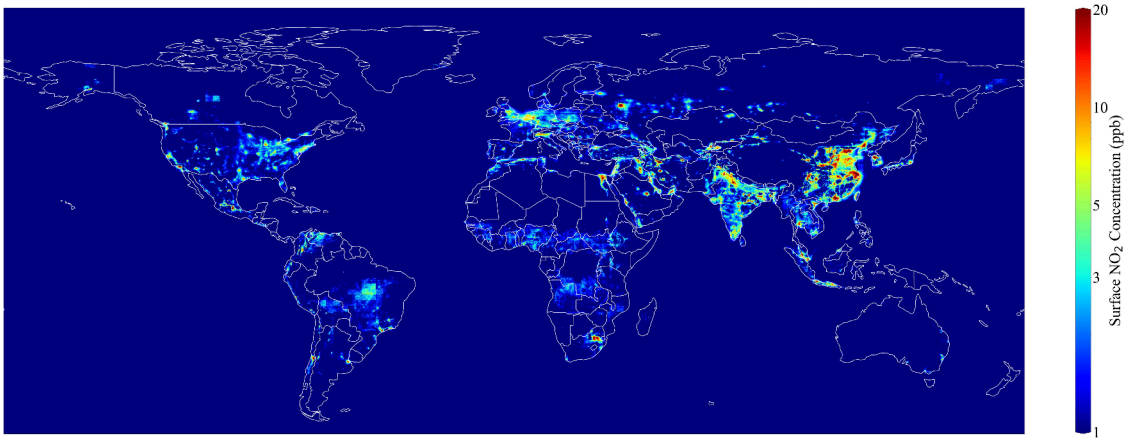

Figure 1. Global surface NO_2 concentrations achieved by combining satellite and modeled NO_2 columns according to Cooper et al.[14] and Nawaz et al.[12] The colorbar saturates at a maximum of 20 ppb to showcase the spatial variability in NO_2 concentrations, but the maximum of the data set extends to 88 ppb.

maxima between estimating the surface NO_2 concentration using just the surface model box and the whole boundary layer column. This algorithm distributes the simulated NO_2 column to the finer resolution and converts the column to a surface concentration, as seen by the two respective terms in parentheses. κ_i is then used to scale the value depending on how polluted the simulated column is, correcting for urban-rural biases in the simulated NO_2 column. Due to NO_2's short lifetime, meaning its concentrations are closely tied to NO_x emissions, this bias correction assuages possible inaccuracies in the NO_x emissions inventory that were propagated into the NO_2 concentrations. Because TROPOMI retrieves NO_2 column abundances at around 1:30 pm local time, the time typically associated with the peak in diurnal NO_2 concentrations, there is a bias associated with using these columns for improving the spatial resolution, but we assume this dissipates in the annual average calculation.[13] The column abundance thresholds that we apply globally are determined by best-fit with the Environmental Protection Agency's (EPA) Air Quality System (AQS) surface NO_2 measurement network[15] by comparing the calculated z_i at the monitoring locations to the annual average NO_2 concentration from the EPA monitor and adjusting the κ_i column thresholds until the bias reduction from changing the thresholds was no longer significant.

2.3. Adjoint Modeling for Source Attribution of Health Burdens. GEOS-Chem adjoint is a useful tool for calculating the sensitivity of a scalar model response (i.e., cost function) to numerous model parameters simultaneously.[16,17] The model component responsible for calculating species concentrations over time, henceforth referred to as the forward model, is driven by assimilated meteorological fields from the NASA Global Modeling and Assimilation Office's GEOS-5 database for 2010 at a 2° × 2.5° global horizontal grid with 47 hybrid sigma-layers.[18] The model's NO_x-VOC-O_3 chemistry mechanism includes chemical NO_x production/loss pathways[19] and aerosol thermodynamics,[20,21] and the meteorology determines the rate of physical and photolytic removal processes. Anthropogenic NO_x emissions are from the ECLIPSE v6b emissions inventory forecasted for 2020 (i.e., not including the effects of COVID-19 lockdowns).[5] We apply the relative contributions of gasoline, middle-distillate (diesel), and other surface transportation to total transportation emissions from ECLIPSE v5a.[22] Natural NO_x emissions include biomass burning from the Global Fire Emissions Database (GFED) v3,[23] and soil and lightning emissions from refs 24 and 25, respectively. Biogenic emissions are sourced from the MEGAN v2.1 emissions inventory.[26]

To determine the sensitivity of the global health burdens to NO_x emissions, we use GEOS-Chem adjoint v35n[16] and define the cost function to be the 2019 global health outcomes associated with NO_2 exposure. As the cost function is specific to a certain health outcome, two cost functions must be defined: one for NO_2-associated pediatric asthma incidences and a second for NO_2-associated premature mortalities. Equation 1 serves as the basis for the cost functions ($J = O_h$), where the health data will depend on which health end point is being modeled (either pediatric asthma or premature mortalities). The GEOS-Chem adjoint model is then run with these cost functions to determine their sensitivities to all emissions. To do so, the cost functions are first differentiated with respect to modeled tropospheric NO_2 column vertical levels at each hour to generate adjoint forcings, given here as eq 4:

$$\frac{\partial J}{\partial \Omega_{I,t}} = \left[\sum_{i\in I}\sum_{g\in G} P_i^g B_i^g \kappa_i \left(\frac{\nu_i \Omega_I - \Omega_I^{FT}}{\Omega_I - \Omega_I^{FT}}\right)\left(\frac{S_{NO_2,I}}{\Omega_I}\right)\beta_h e^{\beta_h \Delta z_i}\right] \sum_{L=1}^{TROP} \frac{f_{I,L,t}}{T} \tag{4}$$

where $f_{I,L,t}$ is the conversion factor for grid cell I and vertical layer L at time t, and T is the temporal averaging term. The adjoint model uses these forcings to then calculate sensitivities ($\lambda_{I,t}$) of the global annual health outcomes to NO_x emissions ($E_{I,t}$) at hour t in model grid cell I:

$$\lambda_{I,t} = \frac{\partial J}{\partial E_{I,t}} \tag{5}$$

To do so, the adjoint model calculates the partial derivative of NO_2 concentrations to NO_x emissions using the chain rule, thereby converting the forcing from being with respect to the annual NO_2 column abundance to that with respect to hourly emissions. While the adjoint values themselves are the tangent linear derivatives (gradients) of the cost function, the model states (species concentrations) at each time step from the forward model are saved during the forward simulation and

https://doi.org/10.1021/acsestair.5c00012
ACS EST Air 2025, 2, 700−709

read-in during the adjoint simulation in order to account for the chemically nonlinear relationship between emissions and NO_2.

Using these adjoint sensitivities, we can estimate the global annual NO_2 exposure-associated health benefit contribution (ΔJ_I) due to a uniform 10% reduction in anthropogenic NO_x emissions using a first-order approximation of the relationship between an emissions perturbation and the resulting global annual health burden change. We use a uniform 10% emission reduction to mimic a reasonably achievable reduction scenario that can quantify the health benefits of just removing a tenth of each sector's emissions. While the linearity approximation breaks down for large emission perturbations due nonlinearities in the cost function and NO_2's chemical mechanisms, Nawaz et al.[17] show that adjoint-based estimates (i.e., eq 5 multiplied by an emission magnitude) for small emission perturbations (±50%) do not significantly deviate from direct model calculations. We further attribute this contribution to the NO_x emission sectors present in the ECLIPSE emissions inventory by regridding each model grid cell's ΔJ_I by the fraction of each sector k's NO_x emissions at the ECLIPSE inventory's native 0.5° × 0.5° resolution e to the total annual anthropogenic NO_x emissions in each model grid cell, aggregated temporally to season s:

$$\Delta J_{e,k,s} = \lambda_{I,s} E_{e,k,s} \tag{6}$$

where $\lambda_{I,t}$'s subscripts adjust to the seasonal aggregation ($t \rightarrow s$).

3. RESULTS

3.1. Annual Average NO_2 Surface Concentrations. Global annual average surface NO_2 concentrations calculated from GEOS-Chem and downscaled using tropospheric vertical column densities from TROPOMI to the 0.01° × 0.01° resolution following eq 2 are shown in Figure 1. Given the short lifetime of NO_2, it is necessary to resolve high concentration areas using satellite downscaling for an accurate estimate of the NO_2-associated health burden. We estimate a global population-weighted average surface NO_2 concentration for 2019 of 5.92 ppb, similar to the 6.6 ppb from Anenberg et al.[4] NO_2 concentrations are evaluated with annual-average surface NO_2 concentrations from EPA AQS, Environment and Climate Change Canada's (ECCC) National Air Pollutant Surveillance (NAPS) Program,[15] and the European Environment Agency (EEA) monitoring networks,[27] and Table 1 summarizes this evaluation (details are provided in the Supporting Information). The modeled concentrations align well with US and Canadian monitored annual-average NO_2 concentrations (mean bias of 0.15 and 0.07 ppb, respectively) but underestimate annual-average concentrations at EEA monitoring locations (mean bias of 3.59 ppb). Without applying the satellite downscaling, the population-weighted mean surface NO_2 concentration drops to 2.46 ppb, and the mean biases in comparison to the AQS, NAPS, and EEA networks increase to 3.93, 3.49, and 5.45 ppb, respectively, emphasizing the importance of satellite downscaling in improving our burden estimates.

Table 1. Model Evaluation of Satellite-Downscaled Surface NO_2 Concentrations against Ground-Level Monitors

Statistic	EPA AQS	ECCC NAPS	EEA	Combined
Mean Bias (ppb)	0.15	0.07	3.59	2.81
Norm. Mean Bias (%)	1.84	1.06	35.8	29.5
RMSE (ppb)	4.37	3.64	3.29	3.82
R^2	0.50	0.49	0.27	0.26

3.2. Pediatric Asthma Burden Associated with NO_2 Exposure Globally in 2019. We estimate that 2.07 (95% CI 0.91−2.70) million pediatric asthma cases are associated with NO_2 exposure globally in 2019, corresponding to 8.12% (95% CI 3.59−10.6%) of the total global burden. Figure 2a shows the aggregated NO_2 exposure-attributed pediatric asthma burdens for each country (see Table S1 for individual country values). Our study is the first to utilize satellite downscaling with a chemical transport model to calculate this health burden, but a few previous studies have quantified these health burdens using different methodologies. Anenberg et al.[4] use a different population database that provides different age ranges, where their data set for the oldest cohort spans ages 15 through 18, and WorldPop includes ages 15 through 19, leading to their smaller burden estimate of 1.85 million. Moreover, their finer 0.0083° × 0.0083° horizontal resolution most likely captures some finer gradients in NO_2 concentrations that our slightly coarser resolution does not, possibly leading to the smaller estimate. Nonetheless, our fraction of the total all-cause burden associated with NO_2 exposure is very similar to this previous study's, underscoring the similarity in the health data and exposure estimates between our approaches.

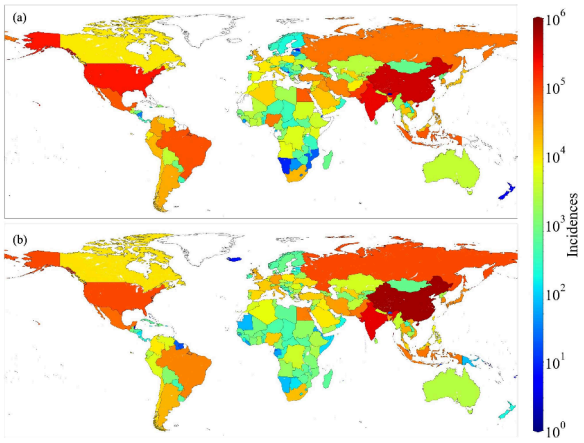

Figure 2. Country-level (a) pediatric asthma and (b) premature death incidences in 2019 associated with long-term NO_2 exposure. Excluded regions (white outlines) are either lacking health data from the GBD study (e.g., Western Sahara) or have annual surface NO_2 concentrations below the counterfactual (e.g., Somalia and Iceland).

In an older study, Achakulwisut et al.[3] associate 4.0 million pediatric asthma cases with NO_2 exposure in 2015, which is almost double what this work and ref 4 found. The main reason, as pointed out in ref 4, is that NO_2 concentrations in rural areas were overestimated using their LUR data set. This led to NO_2 concentrations readily exceeding the 2 ppb counterfactual in many rural regions globally, incorrectly biasing the global burden due to the inflated exposures. We also note further discrepancies between our works, particularly the different years used for the GBD baseline rates, the year of the GBD study (we use 2021, whereas theirs was the 2015 study), and the fact that NO_2 exposures are not constant between years, lead to differences in our global NO_2-associated pediatric asthma burden.

https://doi.org/10.1021/acsestair.5c00012
ACS EST Air 2025, 2, 700−709

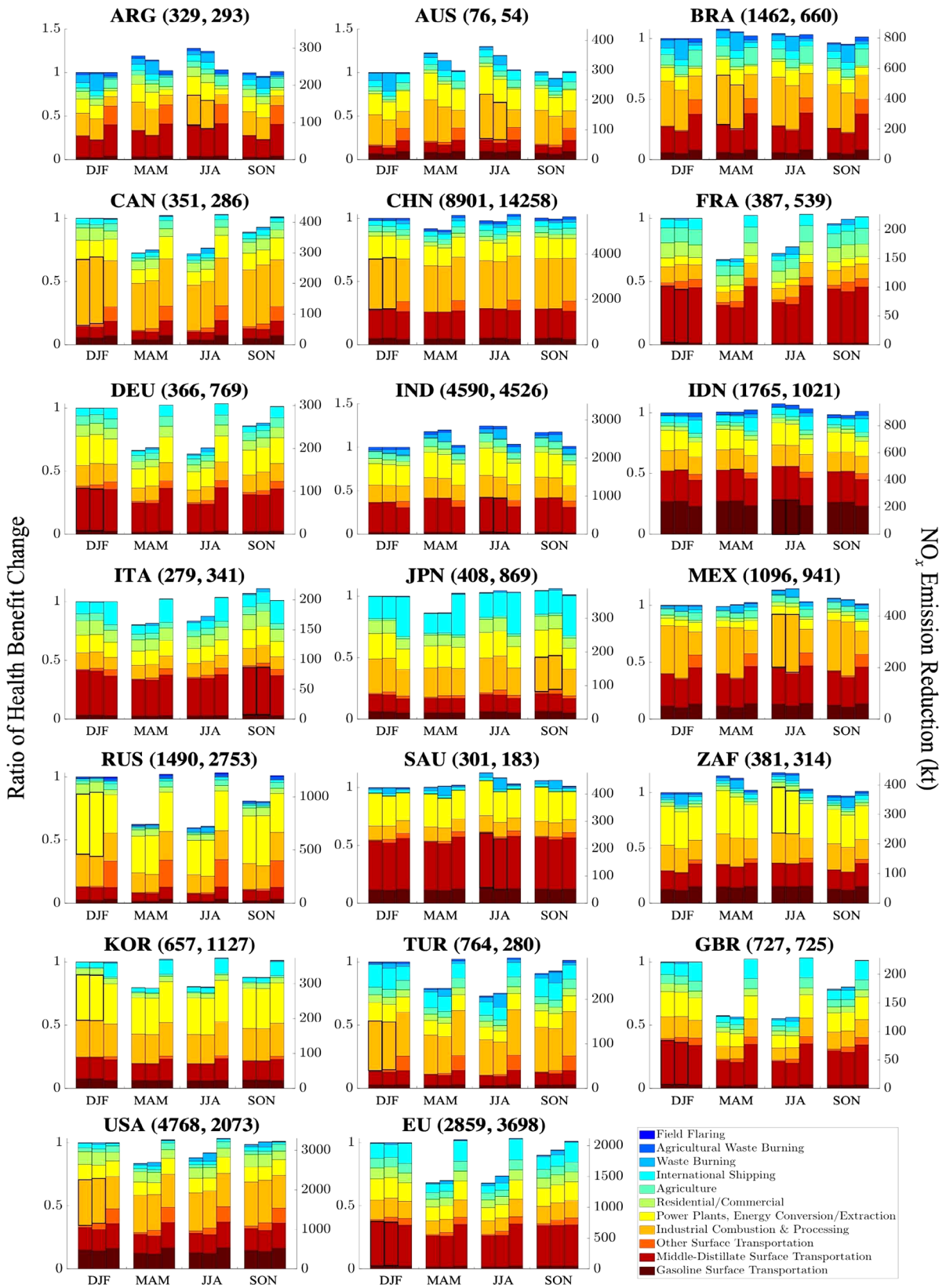

Figure 3. NO_2-associated pediatric asthma (left columns) and premature death (middle columns) health benefits due to 10% NO_x emission reduction as a ratio with respect to DJF (ΔJ) and the total anthropogenic NO_x emission reduction (ΔE, right columns) in each season for each G20 country. DJF's columns are set to the same vertical scale to emphasize the temporal changes in burden reductions and emissions in subsequent seasons. The health benefit corresponding to DJF for pediatric asthma and premature death are given in parentheses after the country name, respectively. The bold sector in each country corresponds to the most efficient sector and season in which to achieve the greatest health benefit due to a 10% reduction in that sector's NO_x emissions. For a list of country names and their associated three-letter abbreviation (the labels used here), see Table S1.

https://doi.org/10.1021/acsestair.5c00012
ACS EST Air 2025, 2, 700−709

3.3. Premature Deaths Associated with NO_2 Exposure Globally in 2019. We estimate 1.98 (95% CI 0.52−2.86) million deaths are associated with NO_2 exposure globally in 2019, corresponding to 4.11% (95% CI 1.09−5.94%) of the total burden. Figure 2b shows the aggregated NO_2 exposure-attributed premature death burdens for each country (see Table S1 as well for individual country values). Whereas our pediatric asthma burden estimate can be directly compared to Anenberg et al.,[4] our NO_2-associated global death estimate is a novel value and therefore lacks being a clear comparison for evaluation. Song et al.[28] estimate an urban NO_2-associated death burden of 549,715 (95% CI 276,204−815,023) deaths using the World Health Organization-recommended NO_2 exposure standard as the counterfactual (10 $\mu g/m^3$, 5.32 ppb), which has the effect of screening-out rural and small urban areas and explains the lower global health burden compared to ours, but the decision to use a counterfactual at all for NO_2-associated mortalities is controversial due to no exposure level being considered "safe".[1,29] Sun et al.[30] estimate 461,301 (95% CI 69,973−843,996) premature deaths were associated with NO_2 exposure globally using an ensemble machine learning model to predict global NO_2 concentrations with good accuracy (their mean absolute error (MAE): 2.68 ppb, RMSE: 4.17 ppb; our MAE: 4.03 ppb, RMSE: 3.82 ppb) but with the same large counterfactual, and therefore discrepancy, as the prior study. Additionally, their coarser horizontal resolution (0.25° × 0.25°) complicates a comparison to ground-based monitors due to the assumption that a monitor's concentration is constant over an entire grid cell, which may also lead to overfitting of urban areas in the training phase where subgrid variability in NO_2 concentrations is large.

Our health burden values also align better with regional studies than those of Sun et al.[30] Camilleri et al.[31] associate 170,850 annual mortalities with NO_2 exposure for the continental United States, where for the same geographic region, we find 95,084 incidences, and Song et al.[28] and Sun et al.[30] only find 38,483 and 15,215, respectively. The discrepancy between our value and those of Camilleri et al.[31] most likely comes from the positive rural bias in the LUR-based NO_2 concentration data set they used,[32] which leads to an overestimate of the national burden given the lack of a counterfactual includes all exposure values in the burden calculation. On a similar note, the controversial use of a counterfactual by Song et al.[28] and Sun et al.[30] is what most likely leads to their significantly lower US estimate compared to ours and Camilleri et al.[31] Khomenko et al.[33] provide a value of 79,435 annual preventable mortalities associated with NO_2 exposure in EU cities if NO_2 concentrations dropped to 3.5 $\mu g/m^3$, a scenario similar to applying a counterfactual to the concentrations, which we interpret as a low-end estimate for the EU burden. Our value for the EU NO_2 exposure-associated death burden in 2019 is 78,996, which is justified by the fact that the former value is a lower bound; we include exposure in rural areas, and our surface NO_2 concentrations are biased low according to the EEA network. Sun et al.[30] find 30,762 mortalities in the EU associated with NO_2 exposure, further showing our method's ability to better match the values presented by previous regional studies.

3.4. Health Benefits Source Attribution. The adjoint model calculations produce model grid-scale estimates of the marginal benefits for reductions in daily NO_x emissions (see Figure S8), which we rescale to the finer ECLIPSE inventory resolution for each economic sector. Here, we present the health benefits associated with a 10% reduction in anthropogenic NO_x emissions aggregated by country and season. We focus on the G20 countries due to their dominant contribution to global NO_x emissions, as well as NO_2-associated pediatric asthma cases and premature mortalities (65%, 66%, and 74% of their respective global totals). We note that the EU (for ease of comparison with previous works, we include the United Kingdom) is not a country; for simplicity, we will refer to all G20 members as "countries" in this work. Figure 3 presents these results by sector as ratios relative to the first season's (DJF) total respective burden alongside the NO_x emissions themselves.

The sectors in Figure 3 with bold outlines correspond to the most impactful sector and season in which to apply NO_x emission controls. In this case, impactful is defined as the greatest seasonal health benefit achieved in either NO_2-associated pediatric asthma or premature death due to 10% NO_x emission reduction. These were determined by aggregating the gridded $\Delta J_{e,k,s}$ to the country-level and for each season and then ranking them from largest to smallest (see Tables S2 and S3 for all rankings). We choose to highlight the largest $\Delta J_{k,s}$ as opposed to $\lambda_{k,s}$ for each country; otherwise, smaller emission sectors, such as waste burning and field flaring, would dominate a marginal impact ranking because of the high sensitivities associated with low emissions. The high sensitivities associated with low emissions (which typically mean the local NO_2 concentrations are themselves low) come from the health impact function's exponential term as well as the relationship between NO_x emissions and NO_2 concentrations often being more responsive at low emissions levels. Thus, low NO_2 concentrations correspond to large slopes of the cost function (i.e., sensitivities). In this way, the sensitivities are weighted by the magnitude of each sector's emissions, providing the recommendations presented in Figure 3.

Figure 3 presents discrepancies between the sectoral distributions of the health benefits from emissions reductions and the NO_x emission reductions themselves. Russia best exemplifies this, where the largest emissions sector in the country, the Power Plants, Energy Generation/Extraction sector, makes up 31% (1,260 kt/yr) of Russian anthropogenic NO_x emissions. If all Russian anthropogenic NO_x emissions are reduced by 10%, this sector would be responsible for 47.0% (2,140 incidences) of the annual NO_2-associated pediatric asthma health benefit from this emission reduction and 49.2% (4,540 incidences) of the annual mortality health benefit. This discrepancy between emissions and burden reduction can be explained by the proximity of these power generation facilities to population centers, particularly within Moscow. Therefore, for Russia, policies focusing on reducing the NO_x emissions from the Power Plants and Energy Generation/Extraction sector would be most impactful in yielding the greatest health benefits. The opposite is true for emission sectors located outside of population centers, like Russia's Other Surface Transportation sector. Despite this sector making up 21.0% (872 kt/yr) of Russian anthropogenic NO_x emissions, this sector only contributes 0.7% (298 incidences) to the NO_2-associated pediatric asthma health benefit and 1.6% (1,313 incidences) of the mortality health benefit in this 10% anthropogenic NO_x emission reduction scenario. The Other Surface Transportation sector consists of vehicle combustion from mining, construction, forestry, agriculture, and other nonroad vehicles,[34] all of which typically exist outside of

https://doi.org/10.1021/acsestair.5c00012
ACS EST Air 2025, 2, 700−709

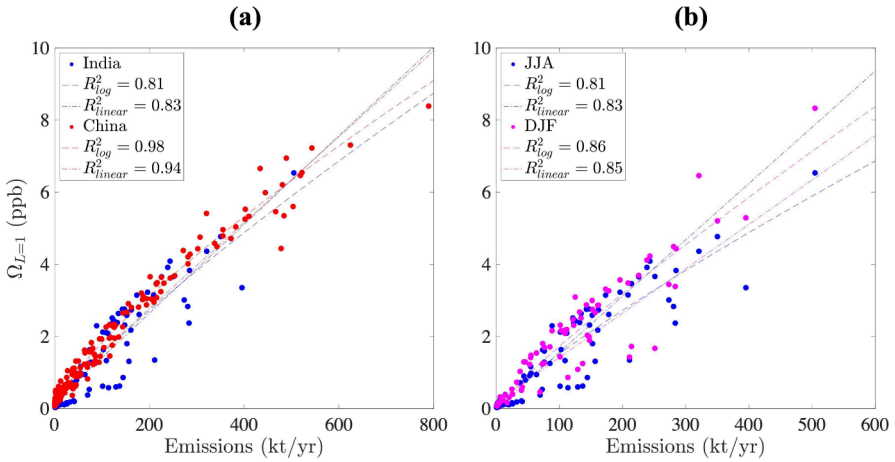

Figure 4. NO_2 concentration vs NO_x emissions plots for (a) India and China in JJA and (b) India in JJA and DJF. R^2 values are adjusted-R^2 for determining best-fit with logarithmic and linear models.

populated areas and therefore exhibit a weak effect on the NO_2 exposure-associated health burden.

Although in many situations they may be more difficult to control than the larger sectors, smaller emission sectors, like the waste burning and field flaring sectors, can still have localized, subnational health impacts. For example, the waste burning sector in Australia, the navy blue sector seen in Figure 3, makes up 1% of national NO_x emission, but when reduced by 10%, the sector is responsible for 4.4% and 12.1% of the annual NO_2-associated pediatric asthma and premature mortality health benefits, respectively. Similar to the Muscovite power plants' influence on Russian health benefits, Australian waste burning by incineration plants is concentrated within urban areas.[35] This results in waste burning NO_x emissions having a more direct influence on NO_2-associated health burdens than more remote emission sectors, such as transportation emissions on rural highways, which results in the large health benefits per unit emission being reduced. Therefore, controls on the Australian waste burning sector would be beneficial in terms of disproportionately large health benefits, but the ultimate impact and feasibility of reducing emissions from smaller sectors, even to near zero, is limited.

For every country, the seasonal variability in health burden reductions exceeds that of NO_x emissions, highlighting the effects of chemical and meteorological variability on the level of NO_2 exposure. Northern hemisphere countries exhibit greater health benefits due to NO_x emission reductions in the colder DJF months, with the opposite being true for the warmer JJA months, and the magnitude of the variability increases with latitude. This pattern is rooted in the lifetime of NO_2 varying with sunlight and temperature: the colder months are those with less energy available for the photolytic NO_2 termination reaction, thereby extending the NO_2 lifetime. This is visible in the seasonality of health benefits between countries like Russia, a country at high latitude, and Saudi Arabia, a country close to the equator, where the health benefit magnitudes have greater seasonal variability in higher-latitude Russia than in Saudi Arabia.

Interestingly, India (along with all South and Southeast Asian countries) exhibits the opposite seasonal trend in health benefits for a northern hemisphere country, where greater health benefits occur during the warmer months (health benefit increases by 20.5% in JJA relative to DJF). To understand this behavior, we consider that the health burden sensitivities with respect to emissions are a product of health burden sensitivities with respect to NO_2 concentrations ($\partial J/\partial C$) and the concentration sensitivities to emissions ($\partial C/\partial E$), and we analyze each separately (see Figure S9). The spatially averaged $\partial J/\partial C$ in India have the same seasonal trend as the contributions due to greater boundary layer heights in JJA than DJF, an expected result for a northern hemisphere country, which means the discrepancy must be in the conversion from the forcing term to the adjoint sensitivity: $\partial C/\partial E$. The relationship between NO_2 concentrations and NO_x emissions follows a somewhat logarithmic trend where low emissions are met with low concentrations and a large slope ($\partial C/\partial E$) due to nonlinear chemistry dominated by photolytic loss of NO_2, and as emissions and concentrations increase, $\partial C/\partial E$ decreases. This relationship is common globally, and Figure 4a shows this phenomenon over China during the summer (JJA) months. In India, however, the photolytic loss associated with traditional "summer" months is superseded by wet deposition during Southeast Asian monsoon season, meaning the nonlinearity of photolytic loss is replaced by first-order wet deposition loss as the more significant loss of NO_2 (via conversion to highly soluble HNO_3 by OH).[36,37] This is shown in Figure 4a, where the R^2 value for China in JJA is larger for fit to a logarithmic model than a linear one, while India's values are fit well by the linear model. This monsoon effect causes the relationship between NO_2 concentrations and NO_x emissions to take on a more linear trend during the JJA monsoon season, leading $\partial C/\partial E$ to increase from its smaller slopes at high concentrations during the logarithmic-trending winter months. The latter is shown in Figure 4b where the R^2 values are slightly higher for the logarithmic model in the nonmonsoon season DJF than in monsoon-affected JJA. Coupled with the larger forcings in JJA than in DJF, this leads to Indian health benefits increasing in JJA compared to DJF.

4. DISCUSSION

4.1. Uncertainties. The GEOS-Chem forward model results derive the most uncertainty from the emission inventories and coarse model resolution. To mitigate the exposure error associated with the coarse 2° × 2.5° horizontal model resolution, TROPOMI NO_2 retrievals are used to downscale each model NO_2 column to a resolution 50,000 times finer that align better with annual-average monitored

https://doi.org/10.1021/acsestair.5c00012
ACS EST Air 2025, 2, 700−709

NO_2 concentrations. However, this downscaling process's parameters were fit using a subset of the ground monitoring data to which we compare, the US EPA AQS, thereby contributing to the high bias seen in the EEA monitors. The same cannot be said for the ECCC NAPS monitors, where bias and error statistics outperformed those of EPA AQS. The adjoint sensitivities are rescaled using the 0.5° × 0.5° sectoral emission magnitudes to improve the spatial resolution; however, the accuracy is limited by the uncertainty in the ECLIPSE emissions inventory.

It is important to note the inconsistency of our meteorological year (2010) in the context of all other model inputs. Our work focuses on the connection between anthropogenic NO_x emissions and the global NO_2 health burden is rather agnostic to the interannual variability of meteorology, given that anthropogenic NO_x emissions are fairly aseasonal and invariant to meteorological variability. Natural emissions only make up 16.1% of total emissions in our model, which equates to only 8.9% of global annual pediatric asthma health benefits and 13.7% of premature deaths' health benefits. Additionally, the downscaling technique we employ uses TROPOMI data from 2019, reducing biases due to the use of 2010 meteorology, and annual differences in transport are not expected to be significant on seasonal time scales given the relatively short atmospheric lifetime of NO_2.

Emissions errors stem from the fact that ECLIPSE v6b forecasts emissions for 2020, which we assume to be unchanged for the year 2019. The forecast modeling was performed in 2015, meaning any influences of COVID-19 lockdowns in 2020 are not present in the inventory for emissions year 2020.[5] However, the predictions made by the inventory were too optimistic in estimating the effect of NO_x emission controls, with the ECLIPSE v6b inventory having been shown to underestimate NO_x emissions when compared to other inventories.[38] We therefore qualify that the presented ΔJ values in Figure 3 are likely an underestimate due to this optimistic forecast, meaning both the NO_2 burden and health benefits from NO_x controls are likely underestimated as well.

In terms of uncertainties in the health impact calculation, the 2019 baseline pediatric asthma and premature death incidence rates are from the GBD 2021 study at the country-level, meaning that the spatial variability of B_i^g within a country is unaccounted for. Previous studies[39] have quantified this error for the US, and while at the state level there were significant deviations, the national health burden changed little (~5.5% difference) between using state-specific and the national average pediatric asthma incidence rates.

Often one of the largest sources of error in air pollution health impact analysis comes from uncertainty in the relative risk values that quantify the association between pollutant exposure and various health end points, including pediatric asthma and premature mortalities.[40] To assess the 95% confidence interval of each NO_2-associated health outcome's 2019 global burden, we perform a global Monte Carlo simulation with n = 1000 relative risk estimates generated by a normal distribution constructed using the central estimates as the means (1.26 for pediatric asthma and 1.04 for premature mortalities), and standard deviations were given by the epidemiological studies (0.05 for pediatric asthma and 0.001 for premature mortality).[1,2] These are then used to build the 95% confidence interval for our global burden estimates (Figure S7). The confidence interval calculated for NO_2 exposure-associated pediatric asthma was smaller than the one for premature mortality, underscoring the greater uncertainty in the latter's estimate. However, these relative risk errors are propagated linearly in the adjoint sensitivity calculation,[41] meaning our recommendation conclusions in Figure 3 would be unchanged.

Skepticism persists regarding the association of NO_2 exposure with premature mortality due to the procedure used in the epidemiological study to determine the relative risk potentially encompassing mortalities associated with exposure to O_3 or $PM_{2.5}$, species which are formed via NO_2 and whose causal associations with long-term health impacts are better established.[9] Values ascribed to NO_2 alone may thus constitute an upper estimate. Nonetheless, the relative risks used in the present work control for exposure to O_3 and $PM_{2.5}$,[1] justifying the presentation of our calculated premature death burden as unique to NO_2. Even if some fraction of the health benefit could ultimately occur via O_3 and $PM_{2.5}$, the cobenefits arising from prevented premature deaths associated with other pollutants nevertheless leads to the intended outcome of improved public health, furthering the utility of implementing our recommended NO_x controls.

4.2. Implications of Implementing NO_x Emission Controls. The recommendations provided in Figure 3 inform each G20 country with the most impactful season and economic sector to control NO_x emissions for the greatest NO_2-associated health benefit, which does not always align with the largest emission sector. Many sectors chosen for the recommendation rank second or third in the emission sector size ranking, emphasizing the importance of our modeling approach in connecting the NO_2 health burdens to the NO_x emissions.

Similar to the country-level results, global NO_x emissions also lack a one-to-one relationship with health benefits. Transportation emissions, responsible for 36% of global NO_x emissions, make up only 28% of the global NO_x emissions, attributable to pediatric asthma and 26% of the mortality health benefits. The opposite is true for the industrial sector (20% of emissions, 23% of both pediatric asthma and mortality health benefits), showing the country-level discrepancies discussed in the results persist at the global level.

Because health burden contribution reductions are the largest during the colder months, policymakers should consider legislation that targets NO_x emissions during the winter. However, this is rarely the case. Current policy regarding NO_x emission reductions[42,43] is preoccupied with reducing surface level O_3 formation during warmer months, meaning the health benefits from reducing NO_2 exposure via NO_x emission controls are not as large as they could be. If these control policies were extended to cover the winter months, the annual health burden associated with NO_2 exposure would be more effectively reduced (e.g., by up to 13% in the US and 38% in the EU for pediatric asthma). It is important to note that these results do not include health burden changes associated with exposure to other pollutants like O_3 and $PM_{2.5}$, meaning that, while the burden associated with NO_2 exposure decreases, this does not guarantee a reduction in burdens associated with exposure to other pollutants. Nonetheless, the case for reducing NO_x emissions is still strengthened by the global deaths of NO_2 exceeding that of O_3, a secondary pollutant whose concentration is directly influenced by the concentration of the former.[44]

https://doi.org/10.1021/acsestair.5c00012
ACS EST Air 2025, 2, 700−709

■ ASSOCIATED CONTENT

Supporting Information

The Supporting Information is available free of charge at https://pubs.acs.org/doi/10.1021/acsestair.5c00012.

Satellite downscaling process using oversampled TROPOMI columns, ECLIPSE v6b NO_x emissions, further evaluation of modeled annual-average surface NO_2 concentrations against ground monitoring networks, baseline incidence rate health data for pediatric asthma and premature death, pediatric asthma and premature deaths associated with NO_2 exposure in 2019 by country, Monte Carlo simulation results for global health burden confidence interval bounds, seasonal sensitivity and forcing calculations, and rankings of absolute and marginal sensitivities for recommendations (PDF)

■ AUTHOR INFORMATION

Corresponding Author

Patrick Wiecko − *Environmental Engineering Program, University of Colorado Boulder, Boulder, Colorado 80303, United States;* orcid.org/0000-0002-5627-3011; Email: patrick.wiecko@colorado.edu

Authors

Daven K. Henze − *Environmental Engineering Program, University of Colorado Boulder, Boulder, Colorado 80303, United States; Department of Mechanical Engineering, University of Colorado Boulder, Boulder, Colorado 80309, United States*

M. Omar Nawaz − *Milken Institute School of Public Health, George Washington University, Washington, D.C. 20037, United States*

Complete contact information is available at: https://pubs.acs.org/10.1021/acsestair.5c00012

Notes

The authors declare no competing financial interest.

■ ACKNOWLEDGMENTS

This work was funded by NASA grants 80NSSC19K0193 and 80NSSC21K1343.

■ REFERENCES

(1) *Systematic Review and Meta-analysis of Selected Health Effects of Long-Term Exposure to Traffic-Related Air Pollution*; Health Effects Institute, 2023.

(2) Khreis, H.; Kelly, C.; Tate, J.; Parslow, R.; Lucas, K.; Nieuwenhuijsen, M. *Environ. Int.* **2017**, *100*, 1−31.

(3) Achakulwisut, P.; Brauer, M.; Hystad, P.; Anenberg, S. C. *Lancet Planetary Health* **2019**, *3*, e166−e178.

(4) Anenberg, S. C.; Mohegh, A.; Goldberg, D. L.; Kerr, G. H.; Brauer, M.; Burkart, K.; Hystad, P.; Larkin, A.; Wozniak, S.; Lamsal, L. *Lancet Planetary Health* **2022**, *6*, e49−e58.

(5) Stohl, A.; et al. *Atmospheric Chemistry and Physics* **2015**, *15*, 10529−10566.

(6) Sagheer, U.; Al-Kindi, S.; Abohashem, S.; Phillips, C. T.; Rana, J. S.; Bhatnagar, A.; Gulati, M.; Rajagopalan, S.; Kalra, D. K. *JACC: Advances* **2024**, *3*, 100805.

(7) Huangfu, P.; Atkinson, R. *Environ. Int.* **2020**, *144*, 105998.

(8) Murray, C. J. L.; et al. *Lancet* **2020**, *396*, 1223−1249.

(9) US EPA Integrated Science Assessment (ISA) for Oxides of Nitrogen - Health Criteria; https://www.epa.gov/isa/integrated-science-assessment-isa-oxides-nitrogen-health-criteria (accessed 07/23/2024).

(10) WorldPop Global 1km Population; https://www.worldpop.org/doi/10.5258/SOTON/WP00647 (accessed 06/03/2024).

(11) Choi, J.; Henze, D. K.; Nawaz, M. O.; Malley, C. S. *GeoHealth* **2024**, *8*, No. e2024GH001042.

(12) Nawaz, M. O.; Henze, D. K.; Harkins, C.; Cao, H.; Nault, B.; Jo, D.; Jimenez, J.; Anenberg, S. C.; Goldberg, D. L.; Qu, Z. *Elementa: Science of the Anthropocene* **2021**, *9*, 00043.

(13) Sun, K.; Zhu, L.; Cady-Pereira, K.; Chan Miller, C.; Chance, K.; Clarisse, L.; Coheur, P.-F.; González Abad, G.; Huang, G.; Liu, X.; Van Damme, M.; Yang, K.; Zondlo, M. *Atmospheric Measurement Techniques* **2018**, *11*, 6679−6701.

(14) Cooper, M. J.; Martin, R. V.; McLinden, C. A.; Brook, J. R. *Environmental Research Letters* **2020**, *15*, 104013.

(15) Demerjian, K. L. *Atmos. Environ.* **2000**, *34*, 1861−1884.

(16) Henze, D. K.; Hakami, A.; Seinfeld, J. H. *Atmos. Chem. Phys.* **2007**, *7*, 2413.

(17) Nawaz, M. O.; Henze, D. K.; Anenberg, S. C.; Braun, C.; Miller, J.; Pronk, E. *GeoHealth* **2023**, *7*, No. e2022GH000713.

(18) Rienecker, M. M.; Suarez, M. J.; Todling, R.; Bacmeister, J.; Takacs, L.; Liu, H.-C.; Gu, W.; Sienkiewicz, M.; Koster, R. D.; Gelaro, R.; Stajner, I.; Nielsen, J. E. The GEOS-5 Data Assimilation System-Documentation of Versions 5.0.1, 5.1.0, and 5.2.0; NASA/TM-2008-104606-VOL-27; 2008.

(19) Jacob, D. J. *Atmos. Environ.* **2000**, *34*, 2131−2159.

(20) Binkowski, F. S.; Roselle, S. J. *Journal of Geophysical Research: Atmospheres* **2003**, *108*, 1.

(21) Nault, B. A.; et al. *Atmospheric Chemistry and Physics* **2021**, *21*, 11201−11224.

(22) ECLIPSE V5a global emission fields - Global Emissions - IIASA; https://iiasa.ac.at/models-tools-data/global-emission-fields-of-air-pollutants-and-ghgs (accessed 07/18/2024).

(23) Van der Werf, G. R.; Randerson, J. T.; Giglio, L.; Collatz, G. J.; Mu, M.; Kasibhatla, P. S.; Morton, D. C.; DeFries, R. S.; Jin, Y.; van Leeuwen, T. T. *Atmospheric Chemistry and Physics* **2010**, *10*, 11707−11735.

(24) Hudman, R. C.; Moore, N. E.; Mebust, A. K.; Martin, R. V.; Russell, A. R.; Valin, L. C.; Cohen, R. C. *Atmospheric Chemistry and Physics* **2012**, *12*, 7779−7795.

(25) Murray, L. T. *Current Pollution Reports* **2016**, *2*, 115−133.

(26) Guenther, A. B.; Jiang, X.; Heald, C. L.; Sakulyanontvittaya, T.; Duhl, T.; Emmons, L. K.; Wang, X. *Geoscientific Model Development* **2012**, *5*, 1471−1492.

(27) European Environment Agency Annual mean NO_2 concentrations; https://www.eea.europa.eu/data-and-maps/figures/annual-mean-no2-concentrations (accessed 07/18/2024).

(28) Song, J.; Wang, Y.; Zhang, Q.; Qin, W.; Pan, R.; Yi, W.; Xu, Z.; Cheng, J.; Su, H. *Science of The Total Environment* **2023**, *866*, 161395.

(29) Qian, Y.; Li, H.; Rosenberg, A.; Li, Q.; Sarnat, J.; Papatheodorou, S.; Schwartz, J.; Liang, D.; Liu, Y.; Liu, P.; Shi, L. *Environ. Health Perspect.* **2021**, *129*, 127009.

(30) Sun, W.; Lu, K.; Li, R. *Environ. Pollut.* **2024**, *359*, 124562.

(31) Camilleri, S. F.; Kerr, G. H.; Anenberg, S. C.; Horton, D. E. *Environ. Sci. Technol. Lett.* **2023**, *10*, 1159−1164.

(32) Larkin, A.; Geddes, J. A.; Martin, R. V.; Xiao, Q.; Liu, Y.; Marshall, J. D.; Brauer, M.; Hystad, P. *Environ. Sci. Technol.* **2017**, *51*, 6957−6964.

(33) Khomenko, S.; Cirach, M.; Pereira-Barboza, E.; Mueller, N.; Barrera-Gómez, J.; Rojas-Rueda, D.; Hoogh, K. d.; Hoek, G.; Nieuwenhuijsen, M. *Lancet Planetary Health* **2021**, *5*, e121−e134.

(34) Klimont, Z.; Kupiainen, K.; Heyes, C.; Purohit, P.; Cofala, J.; Rafaj, P.; Borken-Kleefeld, J.; Schöpp, W. *Atmospheric Chemistry and Physics* **2017**, *17*, 8681−8723.

(35) Tait, P. W.; Brew, J.; Che, A.; Costanzo, A.; Danyluk, A.; Davis, M.; Khalaf, A.; McMahon, K.; Watson, A.; Rowcliff, K.; Bowles, D. *Australian and New Zealand Journal of Public Health* **2020**, *44*, 40−48.

(36) Ghude, S. D.; Fadnavis, S.; Beig, G.; Polade, S. D.; van der A, R. J. *Journal of Geophysical Research: Atmospheres* **2008**, *113*, 1.

(37) Crutzen, P. J.; Lawrence, M. G. *Journal of Atmospheric Chemistry* **2000**, *37*, 81−112.
(38) Jiang, Z.; Zhu, R.; Miyazaki, K.; McDonald, B. C.; Klimont, Z.; Zheng, B.; Boersma, K. F.; Zhang, Q.; Worden, H.; Worden, J. R.; Henze, D. K.; Jones, D. B. A.; Denier van der Gon, H. A. C.; Eskes, H. *Journal of Geophysical Research: Atmospheres* **2022**, *127*, No. e2021JD035872.
(39) Khreis, H.; Alotaibi, R.; Horney, J.; McConnell, R. *Annals of Epidemiology* **2021**, *53*, 76−88.
(40) Ostro, B.; Spadaro, J. V.; Gumy, S.; Mudu, P.; Awe, Y.; Forastiere, F.; Peters, A. *Environmental Research* **2018**, *166*, 713−725.
(41) Henze, D. K.; Seinfeld, J. H.; Shindell, D. T. *Atmospheric Chemistry and Physics* **2009**, *9*, 5877−5903.
(42) US EPA Good Neighbor Plan for 2015 Ozone NAAQS; https://www.epa.gov/Cross-State-Air-Pollution/good-neighbor-plan-2015-ozone-naaqs (accessed 07/08/2024).
(43) Colorado Department of Public Health and Environment State approves bold plan to reduce ozone pollution; https://cdphe.colorado.gov/press-release/state-approves-bold-plan-to-reduce-ozone-pollution (accessed 02/24/2024).
(44) Malley, C. S.; Henze, D. K.; Kuylenstierna, J. C. I.; Vallack, H. W.; Davila, Y.; Anenberg, S. C.; Turner, M. C.; Ashmore, M. R. *Environ. Health Perspect.* **2017**, DOI: 10.1289/EHP1390.

https://doi.org/10.1021/acsestair.5c00012
ACS EST Air 2025, 2, 700−709